

See discussions, stats, and author profiles for this publication at: <https://www.researchgate.net/publication/363331483>

# A Fast and Compact Hybrid CNN for Hyperspectral Imaging-based Bloodstain Classification

Conference Paper · July 2022

DOI: 10.1109/CEC55065.2022.9870277

---

CITATIONS

14

READS

393

5 authors, including:



Muhammad Hassaan Farooq Butt  
University of Electronic Science and Technology of China

13 PUBLICATIONS 38 CITATIONS

[SEE PROFILE](#)



Hamail Ayaz  
ATU Sligo

11 PUBLICATIONS 169 CITATIONS

[SEE PROFILE](#)



Muhammad Ahmad  
National University of Computer and Emerging Sciences

107 PUBLICATIONS 2,082 CITATIONS

[SEE PROFILE](#)

# A Fast and Compact Hybrid CNN for Hyperspectral Imaging-based Bloodstain Classification

Muhammad Hassaan Farooq Butt

School of Computer Science and Engineering,  
and Technology of China.  
Chengdu, Sichuan 611731, China.

Hamail Ayaz

Faculty of Engineering and Design and Centre for  
Precision Engineering, Materials and Manufacturing Research.  
Atlantic Technological University, Sligo, F91 YW50, Ireland.

Muhammad Ahmad

Department of Computer Science,  
National University of Computer  
and Emerging Sciences,  
Chiniot 35400, Pakistan.

Jian Ping Li

School of Computer Science and Engineering,  
University of Electronic Science  
and Technology of China.  
Chengdu, Sichuan 611731, China.

Ramil Kuleev

Research Center for  
Artificial Intelligence  
Innopolis University,  
Innopolis, 420500, Russia.

**Abstract**—In forensic sciences, blood is a shred of essential evidence for reconstructing crime scenes. Blood identification and classification may help to confirm a suspect, although several chemical processes are used to recreate the crime scene. However, these approaches can have an impact on DNA analysis. A potential application of bloodstain identification and classification using Hyperspectral Imaging (HSI) can be used as substance classification in forensic science for crime scene analysis. Therefore, this work proposes the use of a fast and compact Hybrid CNN to process HSI data for bloodstain identification and classification. For experimental and validation purposes, we perform experiments on a publicly available Hyperspectral-based Bloodstain dataset. This dataset has different types of substances i.e., blood and blood-like compounds, for instance, ketchup, artificial blood, beetroot juice, poster paint, tomato concentrate, acrylic paint, uncertain blood. We compare the results with state-of-the-art 3D CNN model and examine the results in detail and present a discussion of each tested architecture with limited availability of the training samples (e.g., only 5% (792 samples) of the data samples are used to train the model, and validated on 5% (792 samples) data samples and finally blindly tested on 90% (14260 samples) of the data samples). The source code can be access on <https://github.com/MHassaanButt/FCHCNN-for-HSIC>

**Index Terms**—Hyperspectral Imaging, Blood Strain Classification, Fast 3D-CNN, Hybird CNN, Forensic Sciences

## I. INTRODUCTION

It is crucial to gather, detect, and analyze evidence from a crime scene as part of a successful and dynamic criminal investigation. Forensic science is the study of true crime cases to collect, detect, and analyze evidence. The types of traces found at a crime scene can be extremely valuable in court investigations as a schematic search, analysis, and conclusions may be drawn [1]–[4]. Body fluids can be one of the most useful forms of forensic evidence found at a crime scene. During violent crime scenes, blood is found in great quantities and is a valuable body fluid [5]. Analyzing bloodstain patterns and determining the age of bloodstains are both important aspects for forensic investigation and can help identify suspects [6], [7].

The first challenge for stain detection at a crime scene is to develop a method to confirm a stain is a bloodstain. Bloodstains can be similar in color and appearance to other substances when visually inspected [8]. It is especially important to select true bloodstains for subsequent DNA testing as false positives, as a brown stain, can lead to a waste of time and resources.

Identification of the dried blood at a scene has become an appealing problem in forensic science [9], and examining the blood spectral components within the skin could serve to estimate the severity of the wound. Methemoglobin (metHB) and oxyhemoglobin (oxyHb) are known as hemoglobin derivatives found in the blood. These derivatives have characteristics peaks in Visible to Infrared (VIS) range spectra, identified as  $\beta \approx 542 \text{ nm}$  and  $\alpha \approx 576 \text{ nm}$ , which could serve to identify the blood or differentiate it from others [10]. In addition, time-induced decay that works on the principle to expose the bloodstain to the elements exhibits the changes in their spectra, this approach could be applied to predict the age of bloodstains [11].

Furthermore, a question arises: How do they behave in images with varying spatial and spectral features (i.e., Hyperspectral Imaging (HSI)), as well as in more difficult scenarios? This work answers these questions by deploying a variety of deep learning architectures and getting to the answers which are more useful from a forensic perspective. To this end, a publically available HSI dataset is being used and can be accessed over [12]. This dataset contains numerous HSI samples, i.e., ketchup, artificial blood, tomato concentrate, poster, and other blood-like substances, like paint (acrylic). This is very difficult to distinguish these samples in traditional images that have visually similar substances. The images in the dataset were acquired at various time intervals to imitate various acquisition settings (laboratory, crime scene, blood splash).

The HSI dataset contains high spectral and low spatial information, thus, traditional as well as 1-D and 2-D Convolutional

Neural Networks (CNNs) are not appropriate because these methods will lose the spatial information and can only process the spectral information. Thus, in order to get benefit from the advantages of both types, such as 3D CNNs, and hybrid (3D followed by 2D CNN) feature hierarchy is used. The objective is to synthesize the competencies of both types of CNNs to refine the spectral-spatial features of HSI that can be used for classification. In order to improve the performance (in terms of computational time) of both CNN models, the HSI cube has been processed through incremental principal component analysis. Later small-sized overlapping 3-D patches are created to process the HSI patches from the 3-D kernel function to create 3D feature maps which preserve the joint spatial and spectral information. Both models are end-to-end, which requires fewer parameters than other 2D/3D CNN models. In addition, a comparative study is performed using recently proposed CNN-based frameworks.

The rest of the paper is structured as follows. Section II discussed state-of-the-art works proposed in the domain of forensic science. Section III presents the methodology used in this work. Section IV provides a detailed description of the experimental dataset, results, and discussion on obtained results. Finally, Section V concludes the paper with possible future research directions.

## II. RELATED WORK

HSI becomes an auspicious tool for forensic science especially in medical diagnosis due to its sensitivity to the hemoglobin [13]–[15] and non-invasive blood detection [16]. Hence, blood detection has been widely studied by the researcher community and some significant research work in the domain of forensic science using HSIs are discussed in this section.

In recent years, bloodstains are identified in forensic labs using different approaches e.g., to identify bloodstains from other confusing substances, several presumptive tests are used. For example, blood can be detected by the Kastle-Meyer (KM) test after a dilution ratio of 1 in 10,000 [17]. However, false positives may occur with the KM test, also known as the phenolphthalein test. A dilution ratio of 1 in 10,000 is also sufficient to detect blood in the Leucomalachite Green (LMG) test [17], though this test is not sensitive as discussed in [18]. The work [19] addressed the fact that LMG is also as sensitive as KM, using a 1 in 10,000 dilution ratio but the KM test is much less sensitive and produces more false negatives than the luminol test [20]. Additionally, the works [21], [22] describes luminol tests that require adequate darkness to process the samples effectively.

For all presumptive tests, confirmatory tests must be conducted to reduce false positives. Spectral, chromatographic, microscopic, and crystallographic analyses can confirm the identity of inorganic materials. In all of these procedures, chemicals are used, or the sample has to be prepared in a way that could create issues for subsequent analysis, such as patterns, and DNA analysis. Additionally, some samples contain a small number of biological trace cases because of

this, the original context can be ruined [23], [24]. Bremmer et. al., [25] uses correlation coefficient in the visible region using reflectance spectroscopy to identify blood. Due to the high absorbance of colored substrates, Edelman et. al., [16] found a problem in identifying blood in the visible region with Near Infrared (NIR) spectroscopy. Since false positives may occur in non-blood substances containing protein, the authors excluded them.

A water peak in the NIR of the method also made it more suitable for dried samples [11]. A supervised pattern recognition technique utilizing NIR spectroscopy was evaluated by Pereira et. al., for identifying human blood [26]. A portable NIR spectrometer was used by Morillas et. al., for the identification of bloodstains. Using different classification models, researchers observed good accuracy of 81-94% [27].

In addition to the NIR, FTIR spectroscopy has been used to differentiate between human and non-human species, for gender identification, and for discriminating between infants and adults. Raman Spectroscopy is also used for both forensics and biomedical applications, while IR technologies are only suited for medical applications such as for IR active substances [28]–[30]. Despite Raman technology's greater potential than IR in forensics, in dried-up samples, its accuracy for forensic work decreases with powered laser light due to the degradation of blood structure. Furthermore, Raman signals are complicated when weak bands are layered over them. This may require an expert analysis [31]. As a result, all of these spectroscopy techniques provide only spectral information about the entire specimen rather than spatial information about the whole observation area. Spatial information facilitates the extraction of information from different samples with different shapes on different backgrounds. The use of spectral imaging for this purpose has been widely adopted, which offers both the advantages of imaging and spectroscopy.

Due to this need for non-destructive methods, forensic work uses non-destructive methods to identify shreds of proof for immediate past [16]. This is achieved by using various non-contact techniques, since, the traditional techniques are unable to cope with the temperature, and humidity issues which must be maintained to avoid blue spectral shift [32]. Due to this, researchers started exploring HSI which helps to identify the blood traces without making contact, thus limiting the risk of contamination or destruction. Moreover, it provides spectral and spatial information on the material under observation. This leads to fewer errors, faster analysis, and quick identification. Therefore, quick data acquisition, no sample preparation, and less work in labs lead to less workload.

Irrespective of spectroscopy mechanism, HSI has been proposed particularly on dark substrates and patterned substrates [33]. Edelman et. al., [34] determined that the bloodstain is visible at only a few wavelengths, and the appearance of bloodstains on a black background has been demonstrated using chemometric techniques and visible high-sensitivity imaging. Moreover, the authors concluded that bloodstain identification using dark substrates is difficult for this range. Li et al. [35] used 415 nm Soret peak as a bloodstain marker which

provides a unique method for bloodstain detection in which they spilled blood on multicolored materials such as red wine or lipstick to identify over visible wavelengths. The work [36] describes how correlation coefficients can be used with the SORET band to determine blooded fingerprints on white tiles and other colored tiles. The work [16] proves that it is possible to assess the age of blood by observing how hemoglobin degradation affects its reflectance spectra. The work [37] examined different clustering algorithms on samples aged up to 200 days for their experiments and conclude that estimating blood age without knowing the acquisition environment can be difficult.

HSI Classification (HSIC) is another area being actively investigated using machine learning models [38]–[40]. The models were based on techniques like Artificial Neural Network (ANN) [41], Support Vector Machine (SVM) [42], and Random Forests [43]. Recently, deep neural networks have gained in popularity as a result of their successful applications in classic image classification [44], [45] and object detection [46]. There are several types of architectures employed for HSIC, including convolution models in one [47], two [48] and three dimensions [49], [50].

Recent years have seen a significant increase in the development of deep learning architectures. The works [39], [51], [52] provides a comprehensive summary of the latest HSIC architectures along with a discussion of the results obtained for several common datasets. There is also a wide comparison of ANN architectures across a number of well-known HSI datasets in [53]. This study was particularly interesting as the authors investigated the impact of data augmentation, transfer learning, and residual learning on classification accuracy with relatively small training sets. Since training labels are often difficult to obtain, learning from a limited training set is a major concern in HSIC [54], [55]. It is common for deep learning to require a large number of labels; therefore, the emergence of architectures designed to reduce these requirements, such as [56] is promising. Hybrid dilated residual networks are another novel, interesting approach presented in [57]. It combines classic machine learning algorithms with deep learning. The authors of [58] presented a hybrid classification method that combines deep learning with an SVM and the work [59] presented a method that combines deep metrics with deep learning.

In the case of stain detection, one needs to develop a method for confirming that the stain on a crime scene is a bloodstain since this is the most difficult part of stain detection. Visual examination of a bloodstain can yield a similar appearance and color to that of other substances [8]. Despite its use in identifying suspects, Deoxyribonucleic Acid (DNA) analysis is time-consuming and highly expensive. If a false positive shows up, as in the case of a brown stain on the screen, much time and resources will be wasted.

### III. METHODOLOGY

HSI data represents cubical information denoted by  $S \in R^{M \times N \times L}$ , where  $S$  is an HSI data with 3-dimensional

spectral-spatial information,  $M$  is width,  $N$  is height, and  $L$  is the number of spectral information as depth/bands. Each spatio-spectral pixel of  $S$  consist of  $L$  spectral points and forms one-hot label vector  $B = (y_1, y_2, y_3, \dots, y_n)$  at  $A_i$  sample, as shown in Fig 1. The HSI system has high intra-class similarities, variability, and overlapping nested regions, and to overcome these issues, incremental principle component analysis (iPCA) is used. iPCA reduces the number of spectral data points while retaining identical spatial data.

To employ image classification algorithms, the HSI cube is partitioned into small overlapping 3D-patches, the truth labels of which are determined by the label of the centering pixel. The entire process is followed by creating neighbour patches  $N_p \in R^{w \times w \times B}$  with spatial window  $(w \times w)$  at centered spatial location  $(x, y)$  [40]. For each  $n$  patches  $(M - (w+1)) \times (L - (w+1))$ , covers the width and height of  $(x - (w-1)/2)$  to  $(x + (w-1)/2)$  and  $(y - (w-1)/2)$  to  $(y + (w-1)/2)$ . The 3D-CNN comprehends the HSI cube by automatically extracting relevant spatial-spectral information using 3D kernels and 3D convolutional procedures. The learned features are further analyzed by activation function, which adds nonlinearity. The functional values are produced by the following equations:

$$D_{i,j,k}^{u,v} = ReLu \left( \sum_{\rho=1}^{s_{u-1}} \sum_{\pi=-\gamma}^{\gamma} \sum_{\lambda=-\eta}^{\eta} \sum_{\omega=-\epsilon}^{\epsilon} Q_{u,v,\rho}^{\pi,\lambda,\omega} \times D_{(u-1),\rho}^{(i+\gamma)(j+\eta)(k+\epsilon)} + b_{u,v} \right) \quad (1)$$

where  $ReLu$  is an activation function,  $b_{u,v}$  represents the bias,  $s_{u-1}$  be the 3-D feature maps at  $(u-1)th$  layer with  $Q_{i,j}$  as depth of the kernel at  $2\pi+1, 2\lambda+1$ , and  $2\omega+1$  be the depth, width and height of the Kernel function. Whereas, in 2D-CNN, convolution happens when the sum of the dot product of the input data and the kernel is computed. To span the entire spatial dimension, the kernel is stridden across the input data. The 2D convolutions are generated by the following equation:

$$D_{i,j}^{u,v} = ReLu \left( \sum_{\rho=1}^{s_{u-1}} \sum_{\pi=-\gamma}^{\gamma} \sum_{\lambda=-\eta}^{\eta} Q_{u,v,\rho}^{\pi,\lambda} \times D_{(u-1),\rho}^{(i+\gamma)(j+\eta)} + b_{u,v} \right) \quad (2)$$

where  $D_{i,j}^{u,v}$  is the final output feature map and other parameters are same as equation 1. In a nutshell, the hybrid CNN model convolutional and kernels are as follows:  $3D_{input} = 9, 9, 15, 1$ .  $3D_{conv} = 8 \times 3 \times 3 \times 7 \times 1$  where  $3 \times 3 \times 7$  are kernel sizes for layer 1, following  $3 \times 3 \times 5$ , and  $3 \times 3 \times 3$  for 3D layer 2, and 3. To get better spatial-spectral feature maps, three 3D convolutional layers are implemented which are then reshaped to 2D convolutional layer to increase the spatial features and form hybride CNN model. The kernel size of  $3 \times 3$  is used and further details are shown in Table I. The total number of trainable parameters of the proposed model is 125,943. The activation function was rectified linear units (ReLUs) which

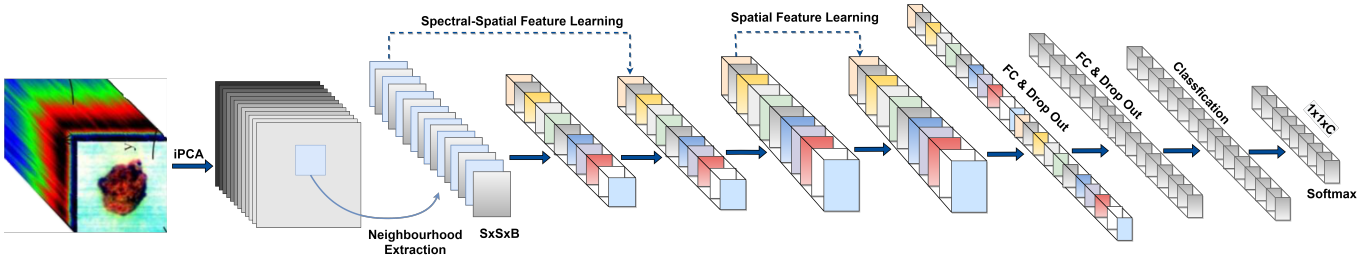


Fig. 1: Hybrid CNN (3D followed by 2D CNN) Model. The layerwise details of each layer is as follows:  $3D_{input} = 9, 9, 15, 1$ .  $3D_{conv} = 8 \times 3 \times 3 \times 7 \times 1$  where  $3 \times 3 \times 7$  are kernel sizes for layer 1, following  $3 \times 3 \times 5$ , and  $3 \times 3 \times 3$  for 3D layer 2, and 3.

is defined as  $f = \max(0, v)$  and the optimizer 'Adam' is used to optimize the soft-max loss function (categorically-cross entropy), and 8 number of epochs are being used to train and validate the model. The convergence loss and accuracy is presented in Figure 2.

TABLE I: The layer wise summary of the proposed Hybrid architecture with window size  $9 \times 9$ .

Layer	Output Shape	# Parameter
Input Layer	$[(9, 9, 15, 1)]$	0
Conv3d_1	$(7, 7, 9, 8)$	512
Conv3d_2	$(None, 5, 5, 5, 16)$	5776
Conv3d_3	$(None, 3, 3, 3, 32)$	13856
Reshape	$(None, 3, 3, 96)$	0
Conv2d	$(None, 1, 1, 64)$	55360
Flatten_1	$(None, 64)$	0
Dense_1	$(None, 256)$	16640
Dropout_1	$(None, 256)$	0
Dense_2	$(None, 128)$	32896
Dropout_2	$(None, 128)$	0
Dense_3	$(None, 7)$	903
Total Trainable Parameters = 125,943		

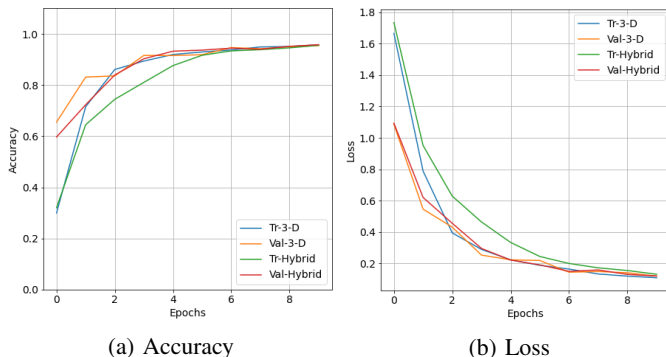


Fig. 2: Convergence lose and accuracy of the Hybrid and 3D CNN models for training and validation data samples.

#### IV. EXPERIMENTAL RESULTS

##### A. Data Set and Experimental Details

HSI Data set used in this study was originally produced and examined by Romaszewski et al., [12]. The HSI dataset contains different fragments of the scene. One sample from them is the scene with different blood-like traces on eight

separate backgrounds, with a mixture of fabric, wood, plastic, and metal and a few of them are red textures. They are a series of stripes and their spectral signatures are shown in Fig 3. Additionally, Fig 4 represents the number of substances, for instance, ketchup, poster paint, acrylic paint, artificial blood, tomato concentration and uncertain blood that resemble very close to the blood traces. More details regarding the dataset can be found in [12].

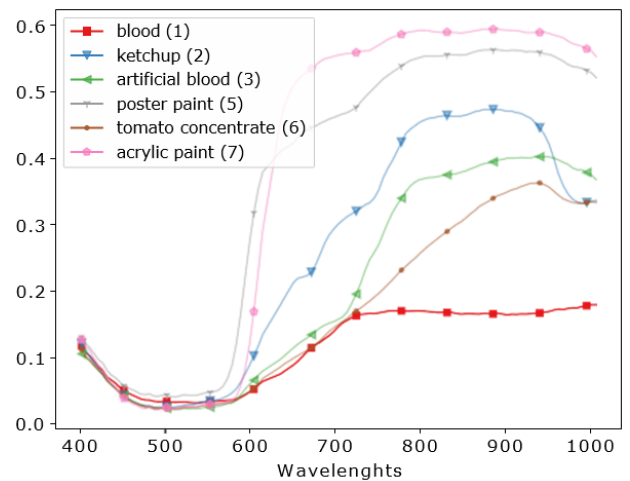


Fig. 3: Spectral signatures of experimental samples (e.g., ketchup, artificial blood, beetroot juice, poster paint, tomato concentrate, acrylic paint, uncertain blood) used in this study.

The entire data set is available online and experimented on an online platform Google Colab. Colab uses online resources to run in any setting and requires a fast internet connection. For data analysis, Colab offers the option of running the algorithms on a python 3 notebook with a graphics processing unit (GPU), 25 GB of random access memory (RAM), and 358.27 GB of cold storage. The experiment is divided into three separate sets (Train/Validation/Test). The entire data is spilt into 10%/90% ratio on which 5% is used for training purposes and 5% is used for validation purpose (i.e.,  $5\% + 5\% = 10\%$ ). The rest of the 90% is considered as a blind set (i.e., test set) for the final evaluation of the models.

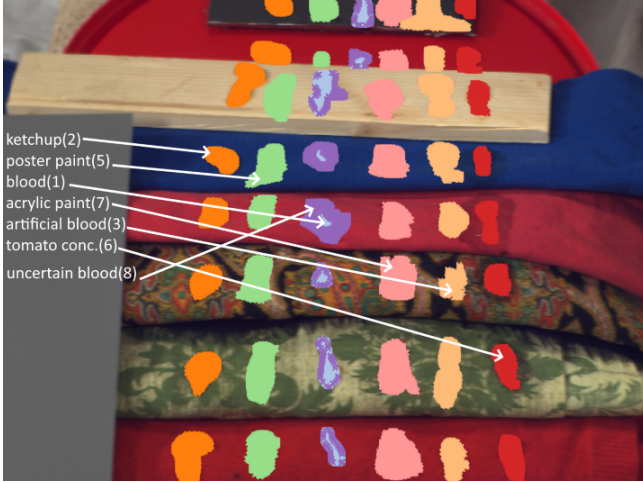


Fig. 4: Substances used to collect the HSI Samples

### B. Classification Results

To validate the claims of the proposed hybrid model, overall accuracy (OA), precision (P), recall (R), and F1score (F1) are computed while training the model using 0.001 as learning rate while training model. The total number of 15 most informative bands are selected using the incremental principle component analysis (iPCA) method. The evaluation achieved by the proposed models has been computed by confusion matrices of E scenario, as shown in Fig 6 and 7. Fig 6 represents the average accuracy (AA) which is 92% is achieved by the fast compact 3D CNN method to classify blood traces from other red hues. Along the AA, the overall accuracy (OA) achieved by this proposed method is 95%. Similarly, Fig 7 also represents the average accuracy (AA) which is 94% is achieved by the hybrid CNN method to classify blood traces from other red hues. Along the AA, the overall accuracy (OA) achieved by this proposed method is 96%. Other statistical results (OA, P, R, F1) is used to evaluate model performance in terms of statistical significance which is shown in table II and table III.

TABLE II: Bloodstain Classification Results using A Fast and Compact 3D CNN Model

Sample	Precision	Recall	F1-score
blood	0.99	0.94	0.97
ketchup	0.98	0.98	0.98
artificial blood	0.89	0.93	0.91
poster paint	1.00	1.00	1.00
tomato concentrate	0.86	0.92	0.89
acrylic paint	0.99	0.94	0.96
<b>Accuracy</b>			0.95
<b>Macro avg</b>	0.95	0.95	0.95
<b>Weighted avg</b>	0.96	0.95	0.95

In comparison to the Hybrid model, the precision achieved by fast 3D-CNN is 95%, however, the precision achieved by the hybrid method is 96%. The higher accuracy achieved by the hybrid model is due to the convergence of the model for an 8 number of epochs, as shown in Fig 2. The observation

achieved from the accuracy and loss curves explains the model convergence at 7 epochs with a limited number of convolutional layers and less number of training samples.

TABLE III: Bloodstain Classification Results using Hybrid Model

Sample	Precision	Recall	F1-score
blood	1.00	0.95	0.97
ketchup	0.98	0.99	0.99
artificial blood	0.88	0.94	0.91
poster paint	0.99	1.00	1.00
tomato concentrate	0.96	0.85	0.90
acrylic paint	0.97	0.97	0.97
<b>Accuracy</b>			0.96
<b>Macro avg</b>	0.96	0.95	0.96
<b>Weighted avg</b>	0.96	0.96	0.96

Furthermore, the graphical maps (i.e., Ground Truths) classification accuracy achieved by the hybrid and 3D CNN is shown in Fig 5. In Fig 5, 5a represent the actual scene from the HSI system, 5b represents the ground truth, 5c presents the classification results achieved by the fast 3D-CNN and 5d shows the accuracy of the proposed hybrid model. In comparison to the state-of-the-art fast 3D-CNN, the Hybrid model outperform to some extent as listed in table III. Additionally, fast 3D-CNN was trained on the parameters and settings as of the Hybrid model except for the 3D to the 2D convolutional layer conversation.

## V. CONCLUSION

In this paper, deep neural networks are employed to classify blood and blood-like substances in hyperspectral images. Experiments were conducted on a relatively new dataset and a series of experiments are performed on this dataset using two different deep learning models. The first one is a fast and compact 3D CNN model which classified substances with an overall precision of 95% having 90% above accuracy to classify each blood-like substance individually. In the other deep learning architecture, we have introduced a hybrid 3D and 2D model for hyperspectral image classification which combines spatio-spectral and spectral information using 3D and 2D convolutions. The Hybrid model sums up complementary information and gives higher accuracy of 96% than fast and compact 3D CNN. The aforesaid models have been compared with a relatively fewer number of training samples i.e., only 5% (792 samples) samples are used to train the models, and validated again on 5% (792 samples) samples. Finally, the trained models are blindly tested on 90% (14260 samples) of the data samples. The possible future research directions include transfer learning while considering the limited availability of training samples to train a deep model without data augmentation.

## ACKNOWLEDGEMENT

This research has been financially supported by The Analytical Center for the Government of the Russian Federation (Agreement No. 70-2021-00143 dd. 01.11.2021, IGK 000000D730321P5Q0002)

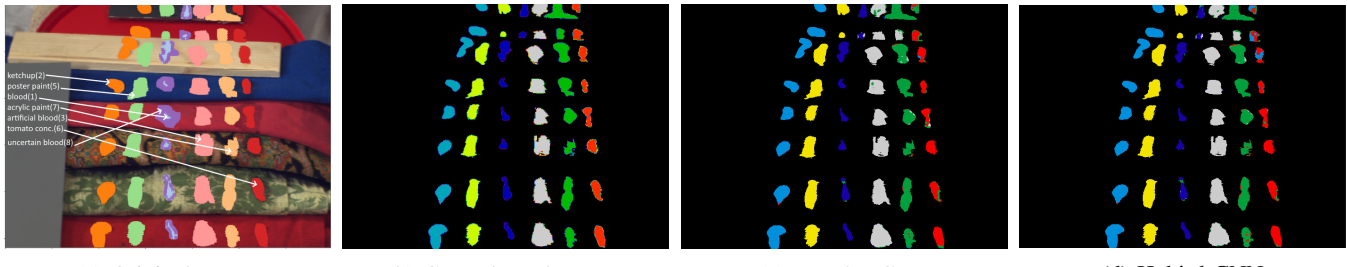


Fig. 5: True image (Fig. 5a), actual Ground Truths (Fig. 5b), Predicted Ground Truths using A Fast and Compact 3D CNN (Fig 5c), and Predicted Ground Truths using Hybrid (3D followed by 2D CNN) CNN (Fig. 5d).

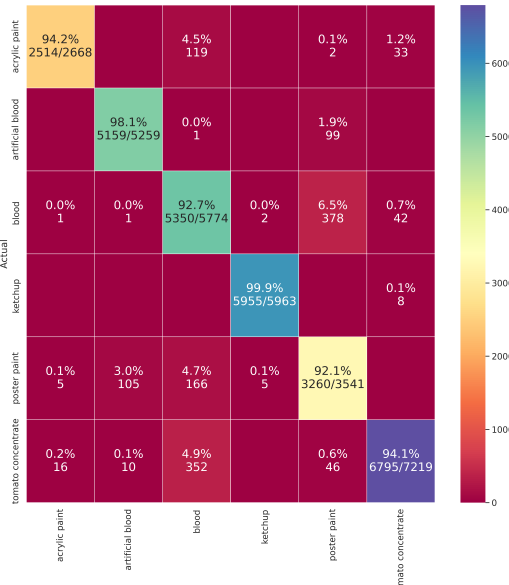


Fig. 6: Confusion matrix using A Fast and Compact 3D CNN Model



Fig. 7: Confusion matrix using Hybrid Model

## REFERENCES

- [1] K. Ksiażek, M. Romaszewski, P. Głomb, B. Grabowski, and M. Cholewa, "Blood stain classification with hyperspectral imaging and deep neural networks," *Sensors*, vol. 20, no. 22, p. 6666, 2020.
- [2] A. C. Doyle, "Methodical approach to processing the crime scene," *An Introduction to Crime Scene Investigation*, pp. 103–133, 2010.
- [3] R. M. Mateen and A. Tariq, "Crime scene investigation in pakistan: a perspective," pp. 285–287, 2019.
- [4] R. M. Morgan, "Conceptualising forensic science and forensic reconstruction. part i: a conceptual model," *Science & Justice*, vol. 57, no. 6, pp. 455–459, 2017.
- [5] E. Mistek, L. Halamoaa, K. C. Doty, C. K. Muro, and I. K. Lednev, "Race differentiation by raman spectroscopy of a bloodstain for forensic purposes," *Analytical chemistry*, vol. 88, no. 15, pp. 7453–7456, 2016.
- [6] S. H. James, P. E. Kish, and T. P. Sutton, *Principles of bloodstain pattern analysis: theory and practice*. CRC press, 2005.
- [7] S. Francesc, *Emerging Technologies for the Analysis of forensic traces*. Springer, 2019.
- [8] A. Y. Wonder, *Bloodstain pattern evidence: objective approaches and case applications*. Elsevier, 2011.
- [9] G. Zadora and A. Menzyk, "In the pursuit of the holy grail of forensic science—spectroscopic studies on the estimation of time since deposition of bloodstains," *TrAC Trends in Analytical Chemistry*, vol. 105, pp. 137–165, 2018.
- [10] J. Yang, J. J. Mathew, R. R. Dube, and D. W. Messinger, "Spectral feature characterization methods for blood stain detection in crime scene backgrounds," in *Algorithms and Technologies for Multispectral, Hyperspectral, and Ultraspectral Imagery XXII*, vol. 9840. International Society for Optics and Photonics, 2016, p. 98400E.
- [11] G. Edelman, V. Manti, S. M. van Ruth, T. van Leeuwen, and M. Aalders, "Identification and age estimation of blood stains on colored backgrounds by near infrared spectroscopy," *Forensic science international*, vol. 220, no. 1-3, pp. 239–244, 2012.
- [12] M. Romaszewski, P. Głomb, A. Sochan, and M. Cholewa, "A dataset for evaluating blood detection in hyperspectral images," *Forensic Science International*, vol. 320, p. 110701, 2021.
- [13] G. Lu and B. Fei, "Medical hyperspectral imaging: a review," *Journal of biomedical optics*, vol. 19, no. 1, p. 010901, 2014.
- [14] H. Ayaz, M. Ahmad, A. Sohaib, M. N. Yasir, M. A. Zaidan, M. Ali, M. H. Khan, and Z. Saleem, "Myoglobin-based classification of minced meat using hyperspectral imaging," *Applied Sciences*, vol. 10, no. 19, p. 6862, 2020.
- [15] H. Ayaz, M. Ahmad, M. Mazzara, and A. Sohaib, "Hyperspectral imaging for minced meat classification using nonlinear deep features," *Applied Sciences*, vol. 10, no. 21, p. 7783, 2020.
- [16] G. Edelman, E. Gaston, T. Van Leeuwen, P. Cullen, and M. Aalders,

- "Hyperspectral imaging for non-contact analysis of forensic traces," *Forensic science international*, vol. 223, no. 1-3, pp. 28–39, 2012.
- [17] R. P. Spalding, "Identification and characterization of blood and bloodstains," in *Forensic Science*. CRC Press, 2002, pp. 209–230.
- [18] W. Lalonde and J. S. Millman, "Case study: Loss of kastle-meyer test specificity on jeans," *Science & Justice*, vol. 59, no. 3, pp. 359–361, 2019.
- [19] E. Johnston, C. E. Ames, K. E. Dagnall, J. Foster, and B. E. Daniel, "Comparison of presumptive blood test kits including hexagon obti," *Journal of forensic sciences*, vol. 53, no. 3, pp. 687–689, 2008.
- [20] F. Barni, S. W. Lewis, A. Berti, G. M. Miskelly, and G. Lago, "Forensic application of the luminol reaction as a presumptive test for latent blood detection," *Talanta*, vol. 72, no. 3, pp. 896–913, 2007.
- [21] D. Nagesh and S. Ghosh, "A time period study on the efficiency of luminol in the detection of bloodstains concealed by paint on different surfaces," *Forensic science international*, vol. 275, pp. 1–7, 2017.
- [22] I. Quinones, D. Sheppard, S. Harbison, and D. Elliot, "Comparative analysis of luminol formulations," *Canadian Society of Forensic Science Journal*, vol. 40, no. 2, pp. 53–63, 2007.
- [23] K. Virkler and I. K. Lednev, "Analysis of body fluids for forensic purposes: from laboratory testing to non-destructive rapid confirmatory identification at a crime scene," *Forensic science international*, vol. 188, no. 1-3, pp. 1–17, 2009.
- [24] P. Thanakiatkrai, K. Raham, J. Pradutkanchana, S. Sothibandhu, and T. Kitpipit, "Direct-str typing from presumptively-tested and untreated body fluids," *Forensic Science International: Genetics*, vol. 30, pp. 1–9, 2017.
- [25] R. H. Bremmer, G. Edelman, T. D. Vegter, T. Bijvoets, and M. C. Aalders, "Remote spectroscopic identification of bloodstains," *Journal of forensic sciences*, vol. 56, no. 6, pp. 1471–1475, 2011.
- [26] J. F. Pereira, C. S. Silva, M. J. L. Vieira, M. F. Pimentel, A. Braz, and R. S. Honorato, "Evaluation and identification of blood stains with handheld nir spectrometer," *Microchemical Journal*, vol. 133, pp. 561–566, 2017.
- [27] A. V. Morillas, J. Gooch, and N. Frascione, "Feasibility of a handheld near infrared device for the qualitative analysis of bloodstains," *Talanta*, vol. 184, pp. 1–6, 2018.
- [28] R. Schalike and M. Illes, "A review of spectroscopic methods applied to bloodstain pattern analysis," *Journal of Multidisciplinary Research at Trent*, vol. 2, no. 1, pp. 90–104, 2019.
- [29] S. Giuliano, E. Mistek-Morabito, and I. K. Lednev, "Forensic phenotype profiling based on the attenuated total reflection fourier transform-infrared spectroscopy of blood: Chronological age of the donor," *ACS omega*, vol. 5, no. 42, pp. 27026–27031, 2020.
- [30] R. Kumar, K. Sharma, and V. Sharma, "Bloodstain age estimation through infrared spectroscopy and chemometric models," *Science & Justice*, vol. 60, no. 6, pp. 538–546, 2020.
- [31] V. Sharma and R. Kumar, "Trends of chemometrics in bloodstain investigations," *TRAC Trends in Analytical Chemistry*, vol. 107, pp. 181–195, 2018.
- [32] E. K. Hanson and J. Ballantyne, "A blue spectral shift of the hemoglobin soret band correlates with the age (time since deposition) of dried bloodstains," *PLoS One*, vol. 5, no. 9, p. e12830, 2010.
- [33] R. L. Schuler, P. E. Kish, and C. A. Plese, "Preliminary observations on the ability of hyperspectral imaging to provide detection and visualization of bloodstain patterns on black fabrics," *Journal of forensic sciences*, vol. 57, no. 6, pp. 1562–1569, 2012.
- [34] G. J. Edelman, T. G. van Leeuwen, and M. C. Aalders, "Visualization of latent blood stains using visible reflectance hyperspectral imaging and chemometrics," *Journal of forensic sciences*, vol. 60, pp. S188–S192, 2015.
- [35] B. Li, P. Beveridge, W. T. O'Hare, and M. Islam, "The application of visible wavelength reflectance hyperspectral imaging for the detection and identification of blood stains," *Science & justice*, vol. 54, no. 6, pp. 432–438, 2014.
- [36] S. Cadd, B. Li, P. Beveridge, W. T. O'Hare, A. Campbell, and M. Islam, "The non-contact detection and identification of blood stained fingerprints using visible wavelength hyperspectral imaging: Part ii effectiveness on a range of substrates," *Science & Justice*, vol. 56, no. 3, pp. 191–200, 2016.
- [37] M. Aalders and L. Wilk, "Investigating the age of blood traces: How close are we to finding the holy grail of forensic science?" in *Emerging Technologies for the Analysis of Forensic Traces*. Springer, 2019, pp. 109–128.
- [38] P. Ghamisi, J. Plaza, Y. Chen, J. Li, and A. J. Plaza, "Advanced spectral classifiers for hyperspectral images: A review," *IEEE Geoscience and Remote Sensing Magazine*, vol. 5, no. 1, pp. 8–32, 2017.
- [39] M. Ahmad, S. Shabbir, S. K. Roy, D. Hong, X. Wu, J. Yao, A. M. Khan, M. Mazzara, S. Distefano, and J. Chanussot, "Hyperspectral image classification—traditional to deep models: A survey for future prospects," *IEEE Journal of Selected Topics in Applied Earth Observations and Remote Sensing*, vol. 15, pp. 968–999, 2022.
- [40] M. Ahmad, A. M. Khan, M. Mazzara, S. Distefano, M. Ali, and M. S. Sarfraz, "A fast and compact 3-d cnn for hyperspectral image classification," *IEEE Geoscience and Remote Sensing Letters*, 2020.
- [41] L. Li, C. Wang, W. Li, and J. Chen, "Hyperspectral image classification by adaboost weighted composite kernel extreme learning machines," *Neurocomputing*, vol. 275, pp. 1725–1733, 2018.
- [42] M. Cholewa, P. Glomb, and M. Romaszewski, "A spatial-spectral disagreement-based sample selection with an application to hyperspectral data classification," *IEEE Geoscience and Remote Sensing Letters*, vol. 16, no. 3, pp. 467–471, 2019.
- [43] Z. Chunhui, G. Bing, Z. Lejun, and W. Xiaoqing, "Classification of hyperspectral imagery based on spectral gradient, svm and spatial random forest," *Infrared Physics & Technology*, vol. 95, pp. 61–69, 2018.
- [44] A. Kolesnikov, L. Beyer, X. Zhai, J. Puigcerver, J. Yung, S. Gelly, and N. Houlsby, "Big transfer (bit): General visual representation learning," in *Computer Vision–ECCV 2020: 16th European Conference, Glasgow, UK, August 23–28, 2020, Proceedings, Part V 16*. Springer, 2020, pp. 491–507.
- [45] K. He, X. Zhang, S. Ren, and J. Sun, "Deep residual learning for image recognition," in *Proceedings of the IEEE conference on computer vision and pattern recognition*, 2016, pp. 770–778.
- [46] Z. Cai, Q. Fan, R. S. Feris, and N. Vasconcelos, "A unified multi-scale deep convolutional neural network for fast object detection," in *European conference on computer vision*. Springer, 2016, pp. 354–370.
- [47] W. Hu, Y. Huang, L. Wei, F. Zhang, and H. Li, "Deep convolutional neural networks for hyperspectral image classification," *Journal of Sensors*, vol. 2015, 2015.
- [48] H. Zhang, Y. Li, Y. Zhang, and Q. Shen, "Spectral-spatial classification of hyperspectral imagery using a dual-channel convolutional neural network," *Remote sensing letters*, vol. 8, no. 5, pp. 438–447, 2017.
- [49] Y. Chen, H. Jiang, C. Li, X. Jia, and P. Ghamisi, "Deep feature extraction and classification of hyperspectral images based on convolutional neural networks," *IEEE Transactions on Geoscience and Remote Sensing*, vol. 54, no. 10, pp. 6232–6251, 2016.
- [50] A. Mohan and M. Venkatesan, "Hybridcnn based hyperspectral image classification using multiscale spatirospectral features," *Infrared Physics & Technology*, vol. 108, p. 103326, 2020.
- [51] M. Paoletti, J. Haut, J. Plaza, and A. Plaza, "Deep learning classifiers for hyperspectral imaging: A review," *ISPRS Journal of Photogrammetry and Remote Sensing*, vol. 158, pp. 279–317, 2019.
- [52] N. Audebert, B. Le Saux, and S. Lefèvre, "Deep learning for classification of hyperspectral data: A comparative review," *IEEE geoscience and remote sensing magazine*, vol. 7, no. 2, pp. 159–173, 2019.
- [53] S. Li, W. Song, L. Fang, Y. Chen, P. Ghamisi, and J. A. Benediktsson, "Deep learning for hyperspectral image classification: An overview," *IEEE Transactions on Geoscience and Remote Sensing*, vol. 57, no. 9, pp. 6690–6709, 2019.
- [54] M. Romaszewski, P. Glomb, and M. Cholewa, "Semi-supervised hyperspectral classification from a small number of training samples using a co-training approach," *ISPRS Journal of Photogrammetry and Remote Sensing*, vol. 121, pp. 60–76, 2016.
- [55] M. Ahmad, A. Khan, A. M. Khan, M. Mazzara, S. Distefano, A. Sohaib, and O. Nibouche, "Spatial prior fuzziness pool-based interactive classification of hyperspectral images," *Remote Sensing*, vol. 11, no. 9, p. 1136, 2019.
- [56] B. Pan, Z. Shi, and X. Xu, "Mugnet: Deep learning for hyperspectral image classification using limited samples," *ISPRS Journal of Photogrammetry and Remote Sensing*, vol. 145, pp. 108–119, 2018.
- [57] F. Cao and W. Guo, "Deep hybrid dilated residual networks for hyperspectral image classification," *Neurocomputing*, vol. 384, pp. 170–181, 2020.
- [58] O. Okuashi and C. E. Ndehedehe, "Deep support vector machine for hyperspectral image classification," *Pattern Recognition*, vol. 103, p. 107298, 2020.

- [59] X. Cao, Y. Ge, R. Li, J. Zhao, and L. Jiao, “Hyperspectral imagery classification with deep metric learning,” *Neurocomputing*, vol. 356, pp. 217–227, 2019.